

CV-QKD with Gaussian and non-Gaussian Entangled States over Satellite-based Channels

Nedasadat Hosseinidehaj and Robert Malaney
School of Electrical Engineering & Telecommunications,
The University of New South Wales,
Sydney, NSW 2052, Australia
neda.hosseini@unsw.edu.au, r.malaney@unsw.edu.au

Abstract—In this work we investigate the effectiveness of continuous-variable (CV) entangled states, transferred through high-loss atmospheric channels, as a means of viable quantum key distribution (QKD) between terrestrial stations and low-Earth orbit (LEO) satellites. In particular, we investigate the role played by the Gaussian CV states as compared to non-Gaussian states. We find that beam-wandering induced atmospheric losses lead to QKD performance levels that are in general quite different from those found in fixed-attenuation channels. For example, circumstances can be found where no QKD is viable at some fixed loss in fiber but is viable at the same mean loss in fading channels. We also find that, in some circumstances, the QKD relative performance of Gaussian and non-Gaussian states can in atmospheric channels be the reverse of that found in fixed-attenuation channels. These findings show that the nature of the atmospheric channel can have a large impact on the QKD performance. Our results should prove useful for emerging global quantum communications that use LEO satellites as communication relays.

I. INTRODUCTION

QKD allows two distant and trusted parties, Alice and Bob, to create a secret key through the use of quantum and classical communications, and can be implemented using discrete-variable (DV) or CV quantum states. In DV-QKD protocols, key information is encoded on the properties of single photons, and in CV-QKD protocols key information is encoded on the quadrature variables of light. In the former technology detection is realized by single-photon detectors e.g., [1]–[3], while in the latter technology detection is realised by more efficient and faster detectors, such as homodyne (or heterodyne) detectors e.g., [4]–[8].

QKD is mostly implemented experimentally in a prepare-and-measure (PM) type scheme e.g., [9], where Alice prepares the quantum states which are then transmitted over an insecure quantum channel towards Bob, who measures the received quantum states, resulting in creation of correlated data between the two trusted parties. Each PM scheme can be represented in an equivalent entanglement-based (EB) scheme, where Alice generates a two-mode entangled state, with one mode being kept by Alice and the other mode being transmitted over an insecure quantum channel. Alice and Bob then proceed to invoke a QKD protocol by measuring their own modes to create correlated data. In both the PM scheme and EB scheme, after generation of the correlated data, Alice and Bob proceed with classical postprocessing including sifting, parameter esti-

mation, reconciliation and privacy amplification over a public (but authenticated) classical channel, to generate a secret key even in the presence of Eve (a potential eavesdropper).

CV-QKD protocols using Gaussian resources have been well analysed in theory and experimentally implemented e.g., [6]–[9]. In the Gaussian PM scheme [6], [7], [9], the prepared quantum states are either coherent states or squeezed states which are modulated by Gaussian distributions. Each Gaussian PM scheme can be represented by an equivalent EB scheme [6]–[8] in which Alice generates a two-mode squeezed vacuum (TMSV) state. Although Gaussian quantum states are a well-established resource from both a theoretical and an experimental perspective (for review see [7]), the use of non-Gaussian states in the implementation of CV-QKD protocols has also garnered interest, e.g. [10]–[13]. Such studies can be motivated in part by the fact that non-Gaussian operations such as photon subtraction [14]–[21] and photon addition [16], [19], [21]–[23] on an incoming TMSV state can lead to higher levels of entanglement [19].

It is widely anticipated that the use of satellites will assist in the deployment of QKD over global scales. Thus, it is important to analyse the effectiveness of CV-QKD protocols over atmospheric channels towards (and from) LEO satellites. Such channels are highly fading in nature since the transmissivity of the channel fluctuates due to atmospheric effects. CV-QKD protocols using Gaussian resources have been studied over atmospheric channels in [24]–[27]. However, works on using non-Gaussian resources in CV-QKD protocols have focussed on fixed-attenuation channels. Thus, it remains unclear whether non-Gaussian entangled states can be effective in the implementation of CV-QKD protocols over atmospheric fading channels (in terms of the quantum key generation rates). The entanglement-generation rate produced by non-Gaussian entangled states passing through atmospheric channels has been recently studied by us [28]. In this present work we extend such studies to consider bounds on the actual quantum key rates generated by such non-Gaussian transfer. We will be particularly interested in comparing such quantum key rates with those arising from Gaussian transfer over atmospheric channels, and Gaussian and non-Gaussian transfer over fixed-attenuation channels.

We will focus on transmission fading caused by the beam wander [24], [29], [30], which is expected to dominate photon

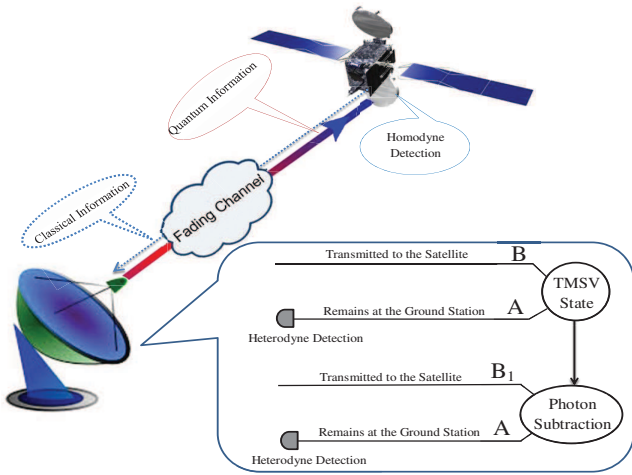


Fig. 1. An example of quantum communication scheme in the ground-to-LEO configuration for implementation of our CV-QKD protocol.

losses in Earth-to-satellite channels. To explore non-Gaussian key generation we will utilize non-Gaussian entangled states which are created just-in-time via photonic subtraction from incoming Gaussian states. In our security analysis, we will include the effects of channel fading, the probabilistic production of the non-Gaussian states, and the most likely imperfections in a CV-QKD protocol (excess noise, inefficient and noisy detectors, and non-perfect reconciliation algorithms). A schematic illustration of the CV-QKD protocol we adopt in a fading uplink configuration is shown in Fig. 1.

The structure of the remainder of this paper is as follows. In Section II, our CV-QKD protocol using a non-Gaussian resource is described, and its security analysis is discussed in detail. In Section III, the performance of the protocol over the atmospheric channels is presented and compared to the corresponding protocol over the fixed-attenuation channels. Finally, concluding results are provided in Section IV.

II. SYSTEM MODEL AND QUANTUM KEY RATE

We now describe the implementation of a CV-QKD protocol using non-Gaussian states and outline how to determine the quantum key rates of this protocol for the atmospheric channel.

A. CV-QKD Protocol using non-Gaussian states

In this work, we will focus on the implementation of a specific CV-QKD protocol in the EB scheme, in which a two-mode non-Gaussian entangled state is shared between Alice and Bob. Initially, we focus on the case where the non-Gaussian state is created just-in-time via photonic subtraction from an incoming Gaussian state - a non-Gaussian operation which has previously been experimentally demonstrated [31], [32].

The protocol begins with Alice possessing a TMSV state, ρ_{AB} , described in the Fock basis as $|TMSV\rangle_{AB} = \sum_{n=0}^{\infty} q_n |n\rangle_A |n\rangle_B$, where $q_n = \lambda^n \sqrt{1 - \lambda^2}$, and where $\lambda = \tanh r$ with r being the squeezing parameter (indices A and

B indicate the two modes). The two-mode squeezing in dB is given by $-10 \log_{10}(\exp(-2r))$. Since the TMSV state is a Gaussian state, it can be completely described by its first moment, which is zero, and its covariance matrix (CM) given by

$$M_{AB}^{in} = \begin{pmatrix} v I & \sqrt{v^2 - 1} Z \\ \sqrt{v^2 - 1} Z & v I \end{pmatrix}, \quad (1)$$

where I is a 2×2 identity matrix, $Z = \text{diag}(1, -1)$, and $v = \cosh(2r)$ is the quadrature variance of each mode. While mode A is held by Alice, the other mode undergoes the photon-subtraction operation. To invoke this operation, Mode B of Alice's TMSV state interacts with a vacuum mode in a beam splitter BS1 with transmissivity T and reflectivity $1 - T$, with one of the outputs of the beam splitter feeding a single-photon detector. When the detector registers one photon, a pure photon-subtracted squeezed (PSS) state is heralded in mode B_1 , the non-measured output of the beam splitter, defined as ρ_{AB_1} , which is a non-Gaussian entangled state. The normalized state arising from this process and its creation probability P_{ss} are given by $|PSS\rangle_{AB_1} = \sum_{n=0}^{\infty} q_n |n+1\rangle_A |n\rangle_{B_1}$, where [19], [28]

$$q_n = (1 - \lambda^2 T) \left(\lambda \sqrt{T} \right)^n \sqrt{n+1}, \quad (2)$$

$$P_{ss} = \frac{\lambda^2 (1 - \lambda^2) (1 - T)}{(1 - \lambda^2 T)^2}.$$

After applying the photon subtraction, the output of the beam splitter, mode B_1 is transmitted towards Bob over an unsecured quantum channel with transmissivity τ . In any real-world implementation of this CV-QKD protocol, the quantum state preparation at Alice's side will produce some additional noise. In the following we refer to this excess noise as ε .

The QKD protocol then proceeds with Bob making a homodyne detection of the amplitude or phase quadrature of the received mode B_2 , and Alice measures both quadratures using a heterodyne detection on mode A to create correlated data.

Bob's realistic homodyne detection will have an efficiency μ and an electronic noise ν_{el} [6], [33]. The efficiency can be modeled by placing a beam splitter BS2 of transmissivity μ before an ideal homodyne detector. This detector's electronic noise can be modeled by an EPR state, ρ_{H_0G} , of quadrature variance ν_d , where $\nu_{el} = (1 - \mu)(\nu_d - 1)$. One input port of the beam splitter BS2 is the received mode B_2 , and the second input port is fed by one half of the EPR state, mode H_0 , while the output ports are mode B_3 (which is measured by the ideal homodyne detector) and mode H . Our CV-QKD protocol using the PSS state is shown in Fig. 2.

Since non-Gaussian states are not completely described by the first and second moments of the quadrature operators, we are not able to quantify the evolution of our PSS state solely through the CM. Thus, we will employ the Kraus representation [34] in order to analyze the evolution of our PSS state through the channel. Considering a quantum state

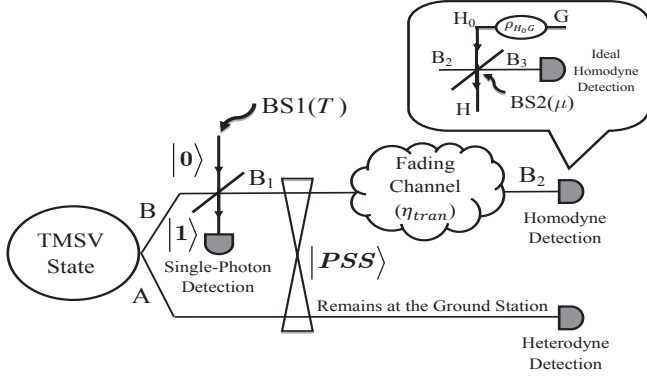


Fig. 2. The entanglement-based CV-QKD protocol over fading channels using the PSS state which is created just-in-time from the incoming TMSV state.

with density operator ρ_{in} as the input of a trace-preserving completely positive channel, the output density operator of the channel can be described in an operator-sum representation of the form $\rho_{out} = \sum_{\ell=0}^{\infty} G_{\ell} \rho_{in} G_{\ell}^{\dagger}$, where the Kraus operators G_{ℓ} satisfy $\sum_{\ell=0}^{\infty} G_{\ell} G_{\ell}^{\dagger} = I$, with I being the identity operator.

The Kraus operators of a fixed-attenuation channel with transmissivity τ can be written as [34],

$$G_{\ell}(\tau) = \sum_{m=0}^{\infty} \sqrt{m+\ell} C_{\ell}(\sqrt{1-\tau})^{\ell} (\sqrt{\tau})^m |m\rangle \langle m+\ell|, \quad (3)$$

where $m+\ell C_{\ell}$ is the binomial coefficient. From these operators it can then be shown that the elementary density operator $|m\rangle \langle n|$ after the evolution through the fixed-attenuation channel can be written as [34],

$$|m\rangle \langle n| \rightarrow \sum_{\ell=0}^{\infty} G_{\ell}(\tau) |m\rangle \langle n| G_{\ell}^{\dagger}(\tau) = \sum_{\ell=0}^{\min\{m,n\}} \sqrt{m C_{\ell}^n C_{\ell}^m} (1-\tau)^{\ell} (\sqrt{\tau})^{(m+n-2\ell)} |m-\ell\rangle \langle n-\ell|. \quad (4)$$

Considering the initial density operator of our PSS state as the following

$$\rho_{AB_1} = \sum_{m=0}^{\infty} \sum_{n=0}^{\infty} q_m q_n |m+1\rangle_A \langle n+1|_A \otimes |m\rangle_{B_1} \langle n|_{B_1}, \quad (5)$$

the density operator of the output mixed state ρ_{AB_2} can be calculated in the Fock basis through the use of Eq. (4), giving

$$\rho_{AB_2} = \sum_{a'=1}^{\infty} \sum_{b'=0}^{\infty} \sum_{c'=1}^{\infty} \sum_{d'=0}^{\infty} \rho_{a'b'c'd'} |a'\rangle_A \langle c'|_A \otimes |b'\rangle_{B_2} \langle d'|_{B_2}, \quad (6)$$

with

$$\rho_{a'b'c'd'} = q_{a'-1} q_{c'-1} \times \sqrt{a'-1} C_{a'-1-b'}^{a'-1} C_{c'-1-d'}^{c'-1} (1-\tau)^{a'-1-b'} (\sqrt{\tau})^{b'+d'} \quad (7)$$

if $a'-b' = c'-d'$ and $a'-1-b' \geq 0$, otherwise $\rho_{a'b'c'd'} = 0$.

We can compute the lower bound on the actual key rate, K , of the protocol by replacing the shared non-Gaussian state between Alice and Bob ρ_{AB_2} with a Gaussian state $\rho_{AB_2}^G$ having the same mean value and CM, resulting in $K(\rho_{AB_2}^G) \leq K(\rho_{AB_2})$. The output mixed state ρ_{AB_2} has zero mean and CM in the following form

$$M_{AB_2} = \begin{pmatrix} x'I & z'Z \\ z'Z & y'I \end{pmatrix}, \quad (8)$$

where

$$x' = \sum_{a'=1}^{\infty} \sum_{b'=0}^{\infty} \sum_{c'=1}^{\infty} \sum_{d'=0}^{\infty} (2a'+1) \rho_{a'b'c'd'} |_{a'=c'}$$

$$y' = \sum_{a'=1}^{\infty} \sum_{b'=0}^{\infty} \sum_{c'=1}^{\infty} \sum_{d'=0}^{\infty} (2b'+1) \rho_{a'b'c'd'} |_{a'=c'}$$

$$z' = \sum_{a'=1}^{\infty} \sum_{b'=0}^{\infty} \sum_{c'=1}^{\infty} \sum_{d'=0}^{\infty} \left(\sqrt{a'b'} \rho_{a'b'c'd'} |_{a'=c'+1} + \sqrt{(a'+1)(b'+1)} \rho_{a'b'c'd'} |_{a'=c'-1} \right). \quad (9)$$

Since the output density operator ρ_{AB_2} possesses an infinite number of elements, we are required to deploy a numerical method to approximate ρ_{AB_2} by limiting its size, i.e. creating a truncated ρ_{AB_2} . Here, a very similar approach to that described in our previous work [28] can be used to estimate ρ_{AB_2} , and then calculate the elements of the CM M_{AB_2} through the use of Eq. (9). However, to determine the true resultant key rates (not just lower bounds) for the non-Gaussian state, Eq. (6) must be utilized.

There is also an analytical approach to obtain the CM M_{AB_2} [11], [12], in which we first need to calculate the CM of the initial PSS state ρ_{AB_1} given by

$$M_{AB_1} = \begin{pmatrix} xI & zZ \\ zZ & yI \end{pmatrix}, \text{ where} \quad (10)$$

$$x = 2v' + 1, \quad y = 2v' - 1, \quad z = 2\sqrt{v'^2 - 1},$$

and where $v' = \frac{1+(1+T)\sinh^2 r}{1+(1-T)\sinh^2 r}$. Note the PSS state ρ_{AB_1} has zero mean.

After transmission of mode B_1 through a quantum channel with transmissivity τ and excess noise ε , the CM of the resulting mixed state ρ_{AB_2} is given by

$$M_{AB_2} = \begin{pmatrix} xI & \sqrt{\tau} z Z \\ \sqrt{\tau} z Z & (\tau(y + \chi_c)) I \end{pmatrix}, \quad (11)$$

where $\chi_c = \varepsilon + \frac{1-\tau}{\tau}$. Note also the numerical method (truncated Eq. (8)) gives effectively the same output CM as the CM in Eq. (11) for $\varepsilon = 0$, provided the output density matrix ρ_{AB_2} is appropriately estimated [28]. After mode B_2 undergoes the beam splitter BS2, the CM of the resulting mixed state ρ_{AB_3} is given by

$$M_{AB_3} = \begin{pmatrix} xI & \sqrt{\mu\tau} z Z \\ \sqrt{\mu\tau} z Z & (\mu\tau(y + \chi)) I \end{pmatrix}, \quad (12)$$

where $\chi = \chi_c + \frac{\chi_d}{\tau}$, and where $\chi_d = \frac{1-\mu}{\mu}\nu_d$. Having the CMs M_{AB_2} in Eq. (11) and M_{AB_3} , we are then able to compute a key rate, which will be a lower bound on the actual key rate of our CV-QKD protocol.

If the original TMSV state ρ_{AB} is exploited as the source of the CV-QKD protocol, the output state at the end of the channel will still be a Gaussian state, whose CM is again given by Eq. (11), but where now x , y and z are given by

$$x = y = v, \quad z = \sqrt{v^2 - 1}. \quad (13)$$

B. Computation of the Secret Key Rate

Here, we summarize some known results in computing a key rate based on the CM of a shared entangled state between the two trusted parties [6], [33]. It is known in the typical point-to-point CV QKD, the reverse reconciliation (RR) scenario always leads to higher key rates than the direct reconciliation (DR) scenario [35]. Hence, we will only consider the RR scenario where Bob's data is the reference of reconciliation. For a realistic reconciliation algorithm, the asymptotic key rate against collective attacks for RR is given by $K = \xi I_{ab_3} - I_E$, where $0 < \xi < 1$ is the reconciliation efficiency, I_{ab_3} is the mutual information between Alice and Bob's measurements after accounting for additional detector noise and efficiencies. I_E is the Holevo quantity, which gives an upper bound on the quantum information stolen by Eve.

We will assume Bob makes the homodyne detection of \hat{q}_{B_3} , the amplitude quadrature of mode B_3 . On the other side, Alice invokes heterodyne detection by combining mode A with a vacuum mode on a balanced beam splitter, and applies homodyne detection on conjugate quadratures of the two output modes. Due to the symmetry between the two conjugate quadratures, we only consider the measurement of the amplitude quadrature of mode A^{he} (one output mode of the balanced beam splitter), which is given by $\hat{q}_{A^{he}} = \frac{1}{\sqrt{2}}(\hat{q}_A + \hat{q}_0)$, where \hat{q}_A is the amplitude quadrature of mode A prior to the heterodyne detection and \hat{q}_0 is the amplitude quadrature of the vacuum input. Then $I_{ab_3} = \frac{1}{2} \log_2 \left(\frac{V_{B_3}}{V_{B_3|A^{he}}} \right)$, where V denotes the variance, and

$$V_{B_3} = \langle \hat{q}_{B_3}^2 \rangle, \quad V_{B_3|A^{he}} = \langle \hat{q}_{B_3}^2 \rangle - \frac{\langle \hat{q}_{B_3}, \hat{q}_{A^{he}} \rangle^2}{\langle \hat{q}_{A^{he}}^2 \rangle}, \quad (14)$$

where $\langle \cdot \rangle$ denotes the expectation value. According to the CM M_{AB_3} in Eq. (12) we will have

$$\begin{aligned} \langle \hat{q}_{B_3}^2 \rangle &= \mu\tau (y + \chi), \\ \langle \hat{q}_{B_3}, \hat{q}_{A^{he}} \rangle &= \frac{1}{\sqrt{2}} \langle \hat{q}_{B_3}, \hat{q}_A \rangle = \frac{1}{\sqrt{2}} \sqrt{\mu\tau} z, \\ \langle \hat{q}_{A^{he}}^2 \rangle &= \frac{1}{2} (\langle \hat{q}_A^2 \rangle + 1) = \frac{1}{2} (x + 1). \end{aligned} \quad (15)$$

Thus, we find $V_{B_3|A^{he}} = \mu\tau \left(y - \frac{z^2}{x+1} + \chi \right)$, which according to the values of x , y and z of the PSS state in Eq. (10) is given by $V_{B_3|A^{he}} = \mu\tau(1+\chi)$. Hence, the mutual information for the CV-QKD protocol using the PSS states is given by $I_{ab_3} = \frac{1}{2} \log_2 \left(\frac{y+\chi}{1+\chi} \right)$.

Eve's information on Bob's measurement outcome, b_3 , is given by $I_E = S(\rho_E) - S(\rho_{E|b_3})$, where $S(\rho)$ is the von Neumann entropy of the state ρ . To determine $S(\rho_E)$ we assume Eve's system ρ_E purifies ρ_{AB_2} , that is, $S(\rho_E) = S(\rho_{AB_2})$. The entropy $S(\rho_{AB_2})$ can be calculated through the symplectic eigenvalues $\nu_{1,2}$ of M_{AB_2} given by Eq. (11). This leads to $S(\rho_{AB_2}) = f(\nu_1) + f(\nu_2)$, where $f(x) = \frac{x+1}{2} \log_2 \left(\frac{x+1}{2} \right) - \frac{x-1}{2} \log_2 \left(\frac{x-1}{2} \right)$, and $\nu_{1,2}^2 = (\Delta \pm \sqrt{\Delta^2 - 4\Omega})/2$, with

$$\begin{aligned} \Delta &= x^2 + \tau^2(y + \chi_c)^2 - 2\tau z^2, \\ \Omega &= (x\tau(y + \chi_c) - \tau z^2)^2. \end{aligned} \quad (16)$$

The second entropy we require in order to determine I_E can be written as $S(\rho_{E|b_3}) = S(\rho_{AHG|b_3})$, since ρ_{AEHG} is pure. The conditional entropy $S(\rho_{AHG|b_3})$ can be calculated as $S(\rho_{AHG|b_3}) = f(\nu_3) + f(\nu_4)$, where

$$\begin{aligned} \nu_{3,4}^2 &= \left(\Delta' \pm \sqrt{\Delta'^2 - 4\Omega'} \right) / 2, \quad \text{with} \\ \Delta' &= \frac{1}{\tau(y+\chi)} \left(\tau(y + \chi_c) + x\sqrt{\Omega} + \chi_d\Delta \right), \\ \Omega' &= \frac{\sqrt{\Omega}}{\tau(y+\chi)} \left(x + \chi_d\sqrt{\Omega} \right). \end{aligned} \quad (17)$$

C. CV-QKD Protocol over Atmospheric Fading Channels

In atmospheric channels the transmissivity η_{tran} fluctuates due to several effects. Such fading channels can be characterized by a distribution of values η , with a probability density distribution $p(\eta)$, where $\eta = \sqrt{\eta_{tran}}$. Consistent with other recent studies [24], [29], [30], we will assume that fading arising from the atmosphere is due only to beam wander. Assuming the beam spatially fluctuates around the center of the receiver's aperture, the probability density distribution $p(\eta)$ can be described by the log-negative Weibull distribution [30],

$$p(\eta) = \frac{2L^2}{\sigma_b^2 \gamma_s \eta} \left(2 \ln \frac{\eta_0}{\eta} \right)^{\left(\frac{2}{\gamma_s} - 1 \right)} \exp \left(- \frac{L^2}{2\sigma_b^2} \left(2 \ln \frac{\eta_0}{\eta} \right)^{\left(\frac{2}{\gamma_s} \right)} \right) \quad (18)$$

for $\eta \in [0, \eta_0]$, with $p(\eta) = 0$ otherwise. Here, σ_b^2 is the beam wander variance, γ_s is the shape parameter, L is the scale parameter, and η_0 is the maximum value of η . The latter three parameters are given by

$$\begin{aligned} \gamma_s &= 8h \frac{\exp(-4h) I_1[4h]}{1 - \exp(-4h) I_0[4h]} \left[\ln \left(\frac{2\eta_0^2}{1 - \exp(-4h) I_0[4h]} \right) \right]^{-1}, \\ L &= \beta \left[\ln \left(\frac{2\eta_0^2}{1 - \exp(-4h) I_0[4h]} \right) \right]^{-(1/\gamma_s)}, \quad \eta_0^2 = 1 - \exp(-2h), \end{aligned} \quad (19)$$

where $I_0[\cdot]$ and $I_1[\cdot]$ are the modified Bessel functions, and where $h = (\beta/W)^2$, with β being the receiver aperture radius and W the beam-spot radius. In our subsequent calculations we will adopt $W = \beta$, and let the mean fading loss be controlled only by adjustments to the value of σ_b .

Since depolarization is very weak in the atmospheric channel, dephasing will also be weak and thus we will ignore it

[36]. We will also assume the transmissivity of the channel can be measured in real-time at the receiver by passing a local oscillator through the channel in an orthogonal polarized mode to the signal.

In the implementation of our CV-QKD protocol over the atmospheric fading channels towards (and from) a LEO satellite, we will assume one mode of the PSS state remains at the ground station (satellite), while the other mode (photon-subtracted mode) is transmitted to the satellite (ground station) over the fading uplink (downlink) with probability density distribution $p(\eta)$. Let us assume Alice is the sender and Bob is receiver. After each realization of η , using the CM in Eqs. (11) and (12), where the transmissivity τ needs to be replaced by η^2 , we can compute the lower bound on the key rate given by $K(\eta)$. Since η is a random variable, the elements of the final key rate is computed by averaging $K(\eta)$ over all possible transmission factors of the fading channel giving $K = \int_0^{\eta_0} K(\eta)p(\eta) d\eta$ in units of bits per pulse.

Note the key rate of the protocol must be computed by including the creation probability P_c of the initial entangled state as $P_c K$. In our protocol, when the PSS state is created just-in-time from the incoming TMSV state, and then used for the CV-QKD protocol $P_c = P_{ss}$. Here, we have assumed the creation probability of the original TMSV state is one.

The range of losses we consider covers a wide range of anticipated scenarios for LEO satellite-based communications with losses in the range 0-10 dB (downlink) to 20-30 dB (uplink). Our results will also be applicable to direct line-of-sight terrestrial communications through air.

III. SIMULATION RESULTS

We now consider the performance of our CV-QKD protocol. In Fig. 3 (top), we plot the key rate $P_c K$ resulting from the PSS states as well as the original TMSV states over the fading channels as a function of channel loss for different values of squeezing of the original TMSV state; 5dB, 10dB and 16dB.¹ As discussed earlier, in this protocol Alice and Bob apply heterodyne detection and homodyne detection, respectively, to their own modes, followed by a RR process. First, we focus on a high-efficiency reconciliation, i.e., $\xi = 0.95$. Our all simulations show the key rate in the presence of several noise sources; the input excess noise of $\varepsilon = 0.01$, and the efficiency and electronic noise of the homodyne detector $\mu = 0.526$ and $\nu_{el} = 0.04361$, respectively [11]. The abscissa of Fig. 3 (top) corresponds to $-10\log_{10}(\int_0^{\eta_0} \eta^2 p(\eta) d\eta)$ and represents the mean fading loss in the fading channel under different conditions (different σ_b). The impact of a low-efficiency reconciliation is investigated in Fig. 4 (top), where we have adopted $\xi = 0.8$. According to the top plots of Fig. 3 and Fig. 4, the computed key rate resulting from the PSS state is always

¹Note for the photon subtraction operation, the transmissivity T of the exploited beam splitter BS1 can be chosen arbitrarily from 0 to 1, leading to the change of the creation probability P_{ss} and also the CM in Eqs. (11) and (12). Thus, for each value of loss, the key rate $P_c K$ varies with different T . Here, in our all simulations we have chosen an optimal value of T for each value of loss to maximise the key rate $P_c K$.

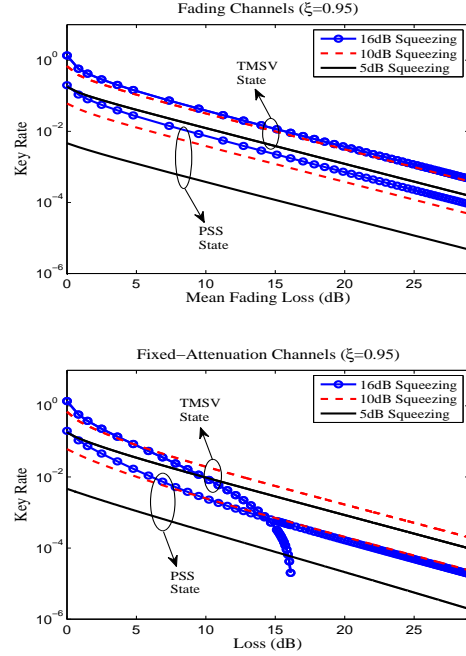


Fig. 3. The key rate (in bits per pulse) over the fading channels (top) and the corresponding fixed-attenuation channels (bottom) using the PSS state and the original TMSV state for different values of initial squeezing with $\xi = 0.95$.

lower than its original TMSV state over the atmospheric fading channels.

We also simulate the performance of our CV-QKD protocol over fixed-attenuation channels. In order to make a valid comparison, we will assume the loss in the fixed-attenuation channel is the same as the mean fading loss in the corresponding fading channel, i.e., $\tau = \int_0^{\eta_0} \eta^2 p(\eta) d\eta$. The bottom plots of Fig. 3 and Fig. 4 show the key rate over the fixed-attenuation channels as a function of channel loss, i.e., $-10\log_{10}(\tau)$ with all the settings and parameters being the same as the corresponding protocols in the top figures. The key rate over the fading channels is always higher than that over the corresponding fixed-attenuation channels. This fact (which comes from the probabilistic nature of the fading channels) is most evident from Fig. 4 where we see the fixed-attenuation channel is not able to generate positive key rates (at high losses) for squeezing of 10dB and 16dB. This is not the case for the corresponding fading channels. From the bottom plots of Fig. 3 and Fig. 4, we can also see that for the high squeezing regime (here 16dB) which is not experimentally achievable at the moment, the PSS state can be more effective in terms of the key rates relative to the original TMSV state for some range of losses (see also [11], [12]).

We have also simulated the performance of the CV-QKD protocol using a state created from the incoming TMSV state by subtracting one photon from *each* mode (using beam splitters with the same transmissivity T). Such a non-Gaussian

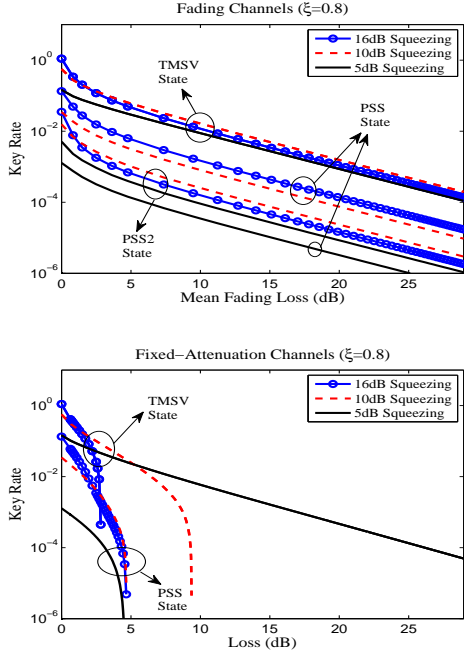


Fig. 4. The key rate (in bits per pulse) over the fading channels (top) and the corresponding fixed-attenuation channels (bottom) using the PSS state, PSS2 state, and the original TMSV state for different values of initial squeezing with $\xi = 0.8$.

state and its creation probability is given by (e.g., [19], [28])

$$|PSS2\rangle = \sum_{n=0}^{\infty} q_n |n\rangle_1 |n\rangle_2, \text{ where}$$

$$q_n = \sqrt{\frac{(1-\lambda^2 T^2)^3}{1+\lambda^2 T^2}} (\lambda T)^n (n+1), \quad (20)$$

$$P_{sb} = \frac{\lambda^2 (1-\lambda^2)(1+\lambda^2 T^2)(1-T)^2}{(1-\lambda^2 T^2)^3}.$$

The CM of the evolved $|PSS2\rangle$ state is again given by Eq. (11) but where now x , y and z are given by

$$x = y = \frac{1 + 3\lambda^4 T^4 + 8\lambda^2 T^2}{1 - \lambda^4 T^4}, \quad z = \frac{4\lambda T (1 + 2\lambda^2 T^2)}{1 - \lambda^4 T^4}. \quad (21)$$

For $|PSS2\rangle$ states over fading channels, we find similar trends to our previous results but with lower key rates (at higher squeezing levels) relative to the single-photon subtracted states. However, the point remains that these new bounds for the $|PSS2\rangle$ states are still less than the TMSV rates. Fig. 4 (top) illustrates this point. Over fixed-attenuation channels the $|PSS2\rangle$ states showed similar trends (not plotted due to closeness of curves).

Finally, we investigate the impact of the imperfect reconciliation process on the resulting key rates (it will suffice to use the TMSV state for this purpose). Fig. 5 (top) shows the key rate K of the CV-QKD protocol achieved by the TMSV state with squeezing 10dB (the state-of-the-art squeezing) as

a function of the reconciliation efficiency ξ and as a function of the fading channel loss. This figure clearly illustrates the negative impact of the imperfect reconciliation process on the resulting key rate. The results shown in the Fig. 5 (bottom) illustrate the key rate K with reconciliation efficiency $\xi = 0.8$ as a function of the initial squeezing of the TMSV state and as a function of the fading channel loss.

According to Fig. 5 (bottom), it is evident that an increase in fading loss reduces the key rate, while increasing the initial squeezing is able to partly compensate the fading's negative effect. However, Fig. 5 (bottom) also shows that a rise in the initial squeezing is not always able to increase the key rate. In fact, for each value of the fading loss there is an optimal value of squeezing which maximizes the key rate. This optimal squeezing is reduced by increasing the fading loss. For instance, for a mean fading loss of 0.8dB, the optimal squeezing is about 15dB, while for higher loss at 11.2dB, the optimal value is around 10dB. Note that in case of perfect reconciliation, i.e. $\xi = 1$, the key rate always grows with the initial squeezing.

Not shown in Fig. 5 is the impact of other real-world issues such as the effect of time delays caused by the reconciliation process (and other such effects). However, the impact of the reconciliation efficiency is in most circumstances the dominant effect in reducing the quantum key rates. State-of-the-art CV reconciliation efficiencies are close to values of 0.95 [37]. At these efficiencies, achievable squeezing levels will produce key rates of 10^{-3} bits per pulse at mean fading loss of 25dB.

IV. CONCLUSION

In this work we have explored the usefulness of Gaussian and non-Gaussian entangled states over atmospheric channels towards LEO satellites. Focussing on the Gaussian component of both types of states as they evolve over the atmospheric channels, we have computed the quantum key rate for the Gaussian case and a lower bound for the non-Gaussian case.

We have also investigated how the presence of noise and imperfections of the protocol affect the key rates. Relative to the corresponding fixed-attenuation channels (such as those found in fiber), we find the fading channels (due to their stochastic nature) can lead to higher key rates. This somewhat counter-intuitive result is most noticeable for the very high-loss channels. We have also found that in some circumstances the non-Gaussian states could result in enhanced quantum key rates over the fixed-attenuation channels compared to the Gaussian states. This is the opposite of what we find in the atmospheric fading channels, once again highlighting the impact the atmosphere can have on the quantum key outcomes. We caution that our rates for the non-Gaussian states are lower bounds - the true key rate for such states remains an open problem. If the bounds shown are here not tight the relative performance levels discussed here may vary.

The role played by the efficiency of the classical reconciliation process, as a function of the mean fading loss and the initial squeezing of the Gaussian states, was also investigated. For state-of-the-art squeezing levels (10dB) and state-

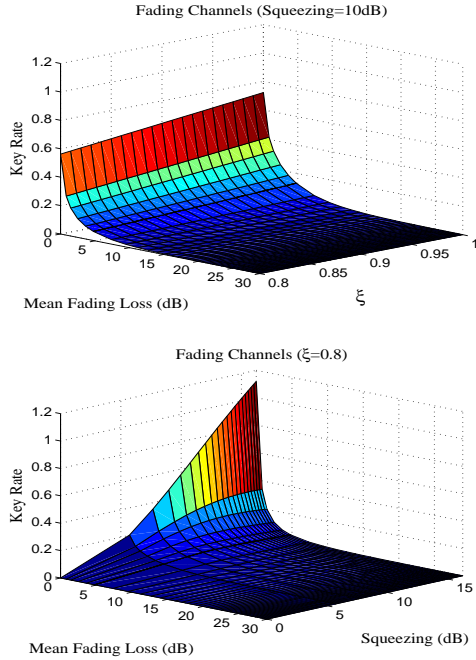


Fig. 5. The key rate (in bits per pulse) over the fading channels using the TMSV state as a function of the mean fading loss and the reconciliation efficiency ξ for squeezing 10dB (top), and also as a function of the mean fading loss and initial squeezing for $\xi = 0.8$ (bottom).

of-the-art reconciliation efficiencies (0.95) we found ground-to-satellite quantum key rates of roughly 10^{-3} bits per pulse are viable. This channel will be the limiting channel in a ground-satellite-ground relay system. Due to the reduced beam wandering losses incurred from space to Earth, the key rates of the satellite-to-ground channels will be roughly an order of magnitude larger.

The calculations presented here should be of value in the quantitative assessment of the CV-QKD protocols using Gaussian and non-Gaussian resources for future quantum communications over atmospheric channels.

REFERENCES

- [1] C. H. Bennett and G. Brassard, "Quantum cryptography: Public key distribution and coin tossing," Proc. of IEEE Int. Conf. on Computers, Systems and Signal Processing, vol. 175, p8, New York, (1984).
- [2] R. Ursin, *et al.*, "Entanglement-based quantum communication over 144km," *Nature Physics* 3, 481 (2007).
- [3] C. Erven, C. Couteau, R. Laamme, and G. Weihs, "Entangled QKD over two free-space optical links," *Opt. Exp.* 16, 21 (2008).
- [4] F. Grosshans, *et al.*, "High-rate quantum cryptography using Gaussian-modulated coherent states," *Nature* 421, 238 (2003).
- [5] V. Scarani, *et al.*, "The security of practical quantum key distribution," *Rev. Mod. Phys.* 81, 1301 (2009).
- [6] R. Garcia-Patron, Ph.D. thesis, Universite Libre de Bruxelles, (2007).
- [7] C. Weedbrook, *et al.*, "Gaussian quantum information," *Rev. Mod. Phys.* 84, 621 (2012).
- [8] C. Weedbrook, "CV QKD with entanglement in the middle," *Phys. Rev. A* 87, 022308 (2013).
- [9] P. Jouguet, *et al.*, "Experimental demonstration of long-distance CV quantum key distribution," *Nature Photonics* 7, 378 (2013).

- [10] A. Leverrier, and P. Grangier, "CV quantum-key-distribution protocols with a non-Gaussian modulation," *Phys. Rev. A* 83, 042312 (2011).
- [11] P. Huang, G. He, J. Fang, and G. Zeng, "Performance improvement of continuous-variable quantum key distribution via photon subtraction," *Phys. Rev. A* 87, 012317 (2013).
- [12] Z. Li, *et al.*, "Non-Gaussian postselection and virtual photon subtraction in CV quantum key distribution," *Phys. Rev. A* 93, 012310 (2016).
- [13] L. F. M. Borelli, L. S. Aguiar, J. A. Roversi, and A. Vidiella-Barranco, "Quantum key distribution using continuous-variable non-Gaussian states," *Quantum Information Processing* 15, 893 (2016).
- [14] T. Opatrny, G. Kurizki, and D.-G. Welsch, "Improvement on teleportation of continuous variables by photon subtraction via conditional measurement," *Phys. Rev. A* 61, 032302 (2000).
- [15] A. Kitagawa, M. Takeoka, M. Sasaki, and A. Chefles, "Entanglement evaluation of non-Gaussian states generated by photon subtraction from squeezed states," *Phys. Rev. A* 73, 042310 (2006).
- [16] Y. Yang and F.-L. Li, "Entanglement properties of non-Gaussian resources generated via photon subtraction and addition and CV quantum-teleportation improvement," *Phys. Rev. A* 80, 022315 (2009).
- [17] S. L. Zhang, and P. van Loock, "Distillation of mixed-state CV entanglement by photon subtraction," *Phys. Rev. A* 82, 062316 (2010).
- [18] K. P. Seshadreesan, J. P. Dowling, and G. S. Agarwal, "Non-Gaussian entangled states and quantum teleportation of Schrodinger-cat states," *Phys. Scr.* 90, 074029 (2015).
- [19] T. J. Bartley and I. A. Walmsley, "Directly comparing entanglement-enhancing non-Gaussian operations," *New Journal of Physics* 17, 023038 (2015).
- [20] T. J. Bartley, *et al.*, "Strategies for enhancing quantum entanglement by local photon subtraction," *Phys. Rev. A* 87, 022313 (2013).
- [21] C. Navarrete-Benlloch, R. Garcia-Patron, J. H. Shapiro, and N. J. Cerf, "Enhancing quantum entanglement by photon addition and subtraction," *Phys. Rev. A* 86, 012328 (2012).
- [22] F. Dell'Anno, S. De Siena, L. Albano, and F. Illuminati, "Continuous-variable quantum teleportation with non-Gaussian resources," *Phys. Rev. A* 76, 022301 (2007).
- [23] S. L. Zhang, Y. Dong, X. Zou, B. Shi, and G. C. Guo, "Continuous-variable-entanglement distillation with photon addition," *Phys. Rev. A* 88, 032324 (2013).
- [24] V. C. Usenko, *et al.*, "Entanglement of Gaussian states and the applicability to quantum key distribution over fading channels," *New Journal of Physics* 14, 093048 (2012).
- [25] B. Heim, *et al.*, "Atmospheric continuous-variable quantum communication," *New Journal of Physics* 16, 113018 (2014).
- [26] N. Hosseini-dehaj and R. Malaney, "Gaussian entanglement distribution via satellite," *Phys. Rev. A* 91, 022304 (2015).
- [27] N. Hosseini-dehaj and R. Malaney, "Quantum key distribution over combined atmospheric fading channels," in Proceedings of IEEE Int. Conf. on Communications (ICC), pp. 7413-7419, (2015).
- [28] N. Hosseini-dehaj and R. Malaney, "Entanglement generation via non-Gaussian transfer over atmospheric fading channels," *Phys. Rev. A* 92, 062336 (2015).
- [29] L. C. Andrews and R. L. Phillips, *Laser Beam Propagation Through Random Media*, 2nd ed. (SPIE, Bellingham, WA, 2005), Vol. PM152.
- [30] D. Yu. Vasylyev, A. A. Semenov, and W. Vogel, "Toward global quantum communication: Beam wandering preserves nonclassicality," *Phys. Rev. Lett.* 108, 220501 (2012).
- [31] H. Takahashi, *et al.*, "Entanglement distillation from Gaussian input states," *Nature Photonics* 4, 178 (2010).
- [32] Y. Kurochkin, A. S. Prasad, and A. I. Lvovsky, "Distillation of the two-mode squeezed state," *Phys. Rev. Lett.* 112, 070402 (2014).
- [33] R. Garcia-Patron and N. J. Cerf, "CV quantum key distribution protocols over noisy channels," *Phys. Rev. Lett.* 102, 130501 (2009).
- [34] J. S. Ivan, K. K. Sabapathy, and R. Simon, "Operator-sum representation for bosonic Gaussian channels," *Phys. Rev. A* 84, 042311 (2011).
- [35] F. Grosshans and P. Grangier, "Reverse reconciliation protocols for quantum cryptography with continuous variables," 6th Int. Conf. on Quantum Communications, Measurement, and Computing, (2002).
- [36] A. A. Semenov, *et al.*, "Homodyne detection for atmosphere channels," *Phys. Rev. A* 85, 013826 (2012).
- [37] M. Shirvanimoghaddam, S. J. Johnson, A. M. Lance "Design of Raptor Codes in the Low SNR Regime with Applications in Quantum Key Distribution," arXiv:1510.07728, (2015).